Structural Study of the Gel Phase of a Semifluorinated Alkane in a Mixed Solvent

Chwen-Yuan Ku*

IPNS, Argonne National Laboratory, Argonne, Illinois 60439

Pierandrea Lo Nostro

Dipartimento di Chimica, Università degli Studi di Firenze, via Gino Capponi 9, 50121 Firenze, Italy

Sow-Hsin Chen

Department of Nuclear Engineering, Massachusetts Institute of Technology, Cambridge, Massachusetts 02139

Received: October 9, 1996[⊗]

Semifluorinated *n*-alkanes, $F_3C(CF_2)_{m-1}(CH_2)_{n-1}CH_3$ (for short, F_mH_n) are short-chain diblock copolymers that show interesting properties when dissolved in nonaqueous media. Due to the high incompatibility between fluorocarbons and hydrocarbons that produces strong immiscibility between fluorocarbons and hydrocarbons, the semifluorinated molecules arrange themselves in peculiar ways both in the solid and in the liquid state. F_mH_n molecules produce micellar aggregates when dispersed in selective solvents such as perfluorooctane or toluene. They form white gel phases when the liquid solution is cooled down below certain temperatures depending on the concentration of the copolymers. These gels are described as a long network of copolymer fibers that entrap free molecules of solvent in cavities formed between different branches of fibers. In this paper we construct two plausible models for the structure of the gel phase of F_8H_{16} dissolved in a mixture of perfluorooctane/isooctane, and we use them to analyze the small-angle X-ray-scattering (SAXS) data. From quantitative analyses of SAXS intensities in absolute scales, we are able to give the values of various structural parameters of the fiber.

Introduction

In spite of their chemical similarity, fluorocarbons and hydrocarbons possess different properties and are immiscible below a certain demixing temperature, as a result of the different chain conformations; in fact $(CH_2)_n$ segments arrange in the usual zigzag conformation with a cross-sectional area of 18.5 Å^2/molecule, whereas a $(CF_2)_m$ chain possesses a typical 15/7 helix conformation and the cross-sectional area is 28.3 Å^2/molecule.[1,2] For this reason fluorocarbon/hydrocarbon mixtures show characteristic phase boundaries (demixing temperature versus either molar or volume fraction) with a broad maximum that corresponds to the upper critical solution temperature (T_c) and to the critical concentration (x_c) or critical volume fraction (ϕ_c).

Semifluorinated *n*-alkanes (or (perfluoroalkyl)alkanes) are diblock short-chain copolymers that show peculiar properties in the liquid and the solid states. They are constituted by two different blocks: a fluorinated chain linked to a hydrocarbon tail $F_3C(CF_2)_{m-1}-(CH_2)_{n-1}CH_3$ (for short, F_mH_n). Since the two segments are covalently bonded, they cannot phase separate.

The presence of both fluorinated and hydrogenated tails in a single semifluorinated alkane molecule produces interesting phenomena in the solid as well as in the liquid state. In the solid state F_mH_n form liquid crystals, show peculiar ordered arrangements, and undergo some phase transitions that have been extensively studied.[3−10]

In spite of the large number of F_mH_n molecules that have been obtained and studied, the properties of the solid state of only few semifluorinated *n*-alkanes have been investigated by birefringence, DSC, SAXS, WAXS, NMR, and Raman spectroscopy. As a matter of fact, these compounds show interesting solid−solid phase transition.

In particular $F_{12}H_n$ molecules show different crystal structure,[8,9] depending on the length of the hydrogenated block (*n*). These semifluorinated *n*-alkanes present two solid−solid phase transitions below the melting temperature.[5] For $4 \leq n \leq 14$, and therefore when $m/n > 1$, the molecular organization of the fluorinated chain is similar to that of fluorinated compounds such as poly(tetrafluoroethylene);[6] when *n* increases the structure of the semifluorinated molecules are less crystalline and more amorphous. For these molecules, the melting points and melting entropies depend only a little on the hydrocarbon chain length, while the solid−solid phase transition strongly depends on *n*. These facts indicate that the melting process basically depends on the fluorinated blocks, and the solid−solid transition is strictly related to the hydrogenated segments.[3,5] NMR experiments confirm that the hydrocarbon tails possess liquid-like conformational freedom and mobility already before the melting point.[3]

When the hydrogenated segment is short ($n = 2, 4, 6$), the small-angle X-ray-scattering (SAXS) profiles show the presence of one sharp peak, with a corresponding spacing that depends on *n* and that is lower than the length of the semifluorinated alkane. In these cases the molecules are tilted with respect to the surface normal for *T* lower than the solid−solid transition temperature (T_c), while they become perpendicular for $T > T_c$. From packing considerations, diffraction densities, and unfavorable fluorocarbon/hydrocarbon interactions, several different structures with some overlapping of the two segments were found to produce scattering profiles like those detected according to the m/n ratio.[8]

For $n = 8, 10, 12$, three to four peaks appear, indicating the presence of two crystal packings that interchange by a sliding

[⊗] Abstract published in *Advance ACS Abstracts,* January 1, 1997.

S1089-5647(96)03120-3 CCC: $14.00 © 1997 American Chemical Society

of the chains along the major molecular axis. For these values of *n*, crystals form lamellar bilayers due to the incompatibility between fluorinated and hydrogenated blocks. The spacing is proportional to the sum of the hydrogenated block length and twice the length of the F_{12} segment. When the H_n block becomes longer, e.g. $F_{12}H_{12}$, the chains are often tilted.[6]

When $n = 14$, 16, 18, and 20, only one single sharp peak and a diffuse maximum appear, which should correspond to a bilayer structure. In particular $F_{12}H_{20}$[3] shows the presence of a bilayered structure with indented hydrogenated blocks.

In the liquid state, semifluorinated alkanes produce micellar aggregates when dissolved in fluorinated or hydrogenated solvents.[5,11−13] Being completely insoluble in water, they also form stable Langmuir monomolecular films and show a slight surface activity at the air/water interface.[14] Heating up a solution containing F_mH_n micellar aggregates results in the destruction of these aggregates, while at lower temperatures the solution forms a gel, depending on the nature of the solvent and on the concentration of the copolymer. These gels are constituted by long fibers of copolymer in an extended network that entraps free solvent molecules. The gels look like soft, high-viscosity materials, which partially dissolve by shaking. By heating up the gel, a clear solution is quickly restored.

F_mH_n solutions in different solvents have been usually studied by several techniques such as static and dynamic light-scattering, NMR, UV absorption, small-angle neutron and X-ray scattering (SANS and SAXS, respectively), differential scanning calorimetry (DSC), surface tension, and dye solubilization measurements. These data clearly show that the copolymer monomers form micellar aggregates, depending on the temperature, on the chemical composition of the F_mH_n, and on the nature of the solvent. The incompatibility between fluorinated and hydrogenated blocks is the main factor that controls the formation of such aggregates. In fact in the presence of a selective solvent, the two blocks will establish different interactions with the solvent molecules and therefore will be confined in different regions of the supramolecular structure.

Since F_mH_n copolymers are able to form aggregates when dissolved in a selective solvent, they have been named as "primitive amphiphiles"; this term refers to an apolar molecule that is formed by two incompatible units and possesses a low dipolar moment. According to this recent definition, primitive amphiphiles represent the ancestors of the whole amphiphiles' family, because of the presence in the same molecule of two incompatible and immiscible moieties, and therefore it is expected that they will provide a useful tool for testing molecular theories of surfactant aggregation.

In a previous paper[1] we reported the results of a study on the F_8H_{16}/perfluorooctane/isooctane three-component system. The addition of even small quantities of F_8H_{16} to a mixture of perfluorooctane (PFO) and isooctane (*i*-OCT) produced a significant lowering of the upper consolute temperature and a relevant broadening of the phase separation curve. Light scattering from the liquid sample was not ascribed to the presence of small aggregates but to a critical scattering related to the demixing of the two solvents.

Larger amounts of copolymer added to the PFO/*i*-OCT system resulted in the formation of a white gel below a certain liquid−gel transition temperature, and in this case no solvent demixing was observed upon cooling. In this high-copolymer state, dynamic light-scattering and SAXS measurements performed on the liquid samples showed the presence of small aggregates characterized by an average hydrodynamic diameter of about 30 Å. Lowering the temperature, the system evolves toward the formation of a bigger structure and eventually to the formation of an extended, ribbon-like sheet.

According to our model for the liquid phase,[1] some copolymer molecules aggregate in the mixed solvent and form small micelles. As the temperature decreases and approaches the liquid−gel phase transition temperature, the original micelles grow and form an extended, ribbon-like structure, where the copolymer molecules produce a lamellar pattern, with the fluorinated chains closely packed in a side-by-side and head-by-head arrangement. The hydrogenated segments will interdigitate in the internal region, given the smaller cross section of the hydrocarbon blocks with respect to the section of the fluorinated helices. As the temperature lowers, other copolymer monomers will be captured and several lamellar layers will be formed, producing birefringent elongated structures that can be observed under a polarizing microscope.

In the present paper we report SAXS experiments performed on the gel phase (at 10, 20, and 30 °C on a sample with a volume fraction of the copolymer $\phi_{COP} \approx 0.60$ and at 20 °C on samples with volume fractions of 0.16, 0.26, and 0.38). We propose two plausible models for the gel phase based on the birefringence picture[1,11] which includes both the fine structure of the crystalline part and the mesoscopic aggregational behavior that leads to the formation of the fibers. We then construct the particle structure factors which approximately describe both the internal structure and the mesoscopic structure of the fibers.

Materials and Methods

Isooctane was purchased from Fluka (Milan, Italy), and perfluorooctane (98%) was supplied by M&G Chemicals (Stockport, England). The solvents were used without further treatment. The semifluorinated *n*-alkane F_8H_{16} was obtained according to the two-step procedure described previously:[13]

$$\text{(i) } F(CF_2)_8I + CH_2{=}CH(CH_2)_{14}H \rightarrow F(CF_2)_8CH_2CHI(CH_2)_{14}H$$

$$\text{(ii) } F(CF_2)_8CH_2CHI(CH_2)_{14}H + H_2 \rightarrow F(CF_2)_8(CH_2)_{16}H$$

Small-angle X-ray-scattering experiments were carried out at the Small-Angle X-Ray-Scattering Facility, Oak Ridge National Laboratory, Oak Ridge, TN. The spectrometer is equipped with a rotating anode X-ray source and a 20 × 20 cm^2 position-sensitive area detector with 64 × 64 pixels. X-rays from Cu Kα line with $\lambda = 1.54$ Å were extracted using a graphite monochromator. The source-to-sample distance was 2 m, with three collimation pinholes, and the resulting beam spot at the sample position is 1.5 mm. The sample-to-detector distance was 2.065 m. This configuration gave us a *Q* range of 0.01−0.25 $Å^{-1}$. The scattering data were corrected for background, detector efficiency, and sample cell scattering. The absolute normalization of the scattering intensity was made with a vitreous carbon standard.

Models of the Gel

The common understanding of the structure of a gel indicates that there are cross-linked long molecules, which constitute a entangled network with cavities. The liquids or solvents fill those cavities to complete the formation of a gel. The cross-linking is often a result of chemical bonding which give rise to a fairly strong network structure in an ordinary gel. This chemical bonding can be hydrogen bonding, solvation, etc..

In our gel samples, there are long fibers grown by successive crystallization of F_8H_{16} copolymers. These long fibers play the role of the long molecules in an ordinary gel so as to form the

porous networks entrapping the liquids among them. The interaction between fibers is considered to be physical contact and the subsequent cross-crystallization or cross-aggregation. Thus the strength of our gel depends on the density of the fibers, since the amount of contact between fibers increases with the density of fibers. The entrapped liquids among the long fibers then contain the rest of the materials in the system which are not involved in the crystallization processes: PFO, *i*-OCT, free F_8H_{16} monomers, and F_8H_{16} micelles formed by the free monomers in the liquids. For the SAXS data analysis, a realistic mathematical model should include all the scattering objects in the samples. Therefore, there are two parts in the model we propose for our gel samples; the first part is the crystal part which comes from the scattering of the F_8H_{16} crystalline networks in the gel, and the second part is the liquid part which accounts for the scattering of micelles in the entrapped liquids.

The scattering patterns we obtained in the experiments are the results of the scattering-length-density contrasts between different domains of the materials. Beside the contrasts inside the crystals and micelles due to the fine structures, there are contrasts between either the crystals or the micelles and the solvents. So it is important to define the solvents in our sample systems. To the crystalline fibers, the solvents are simply the liquids of homogeneous mixture of four components as described above. And to the micelles, the solvents are the homogeneous mixture of three components: PFO, *i*-OCT, and F_8H_{16} monomers.

Define X, the molar ratio of *i*-OCT to F_8H_{16}, and x_1, the PFO molar fraction in the mixtures, according to the phase diagrams of different PFO/*i*-OCT/F_8H_{16} mixtures,[1] for $X = 10$, $T_c \approx 10$ °C. This means at temperatures above 10 °C, for any value of x_1, the mixture is a single-phase liquid or the mixture is homogeneous. For the current samples under investigation, there are two sets of data. One set has data with the volume ratio of PFO to *i*-OCT $r_v = 2.9$ at 10 °C but different F_8H_{16} volume fraction ϕ_{COP}, and another set has data with $r_v = 0.81$ and $\phi_{COP} = 0.6$ but at different temperatures above 10 °C. For $r_v = 2.9$ and $X = 10$, ϕ_{COP} can be calculated to be 7.2%, meaning the mixture will be a one-phase liquid with 7.2% of F_8H_{16} in the mixture. The increase of ϕ_{COP} will decrease X so as to decrease T_c and make the mixture further into the one-phase region. For $r_v = 0.81$ and $X = 10$, $\phi_{COP} = 14.3\%$. Since we know F_8H_{16} form micelles in the single liquid phase, the hypothesis of homogeneous mixture of four or three components can stand if the volume fractions of F_8H_{16} exceed 7.2% and 14.3% for $r_v = 2.9$ and 0.81 data sets, respectively.

Crystal Part. In ref 11, Höpken proposed a cylindrical model for the crystallization of F_mH_n, from both melt and solution on the basis of freeze fracture TEM pictures of $F_{12}H_{20}$ crystals and the fact that the cross sections of fluorocarbon and hydrocarbon segments are different. This model has not been challenged until in ref 1, where we suggested a ribbon model for the networks of F_8H_{16} crystals, which hold the solvents and form a gel phase, to explain the birefringence pictures of the gel.

In this section, we will write down the mathematical formulae for both of the models, and we will compare the results of data analysis using these two different models in next section.

In a small-angle X-ray-scattering experiment, the absolute scattering intensity of a system of independent particles can be expressed as

$$I(Q) = n_p \tilde{P}(Q) \tag{1}$$

where n_p is the particle number density, Q is the magnitude of the scattering wave vector $\vec{Q}$, and $\tilde{P}(Q)$ is the orientationally-averaged particle structure factor. The orientationally-averaged particle structure factor can be expressed as

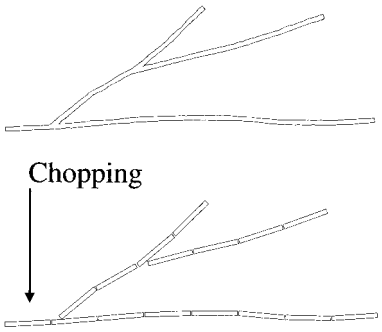

Figure 1. Schematic showing a branched fiber and the results of chopping the fibers into small bricks with straight edges.

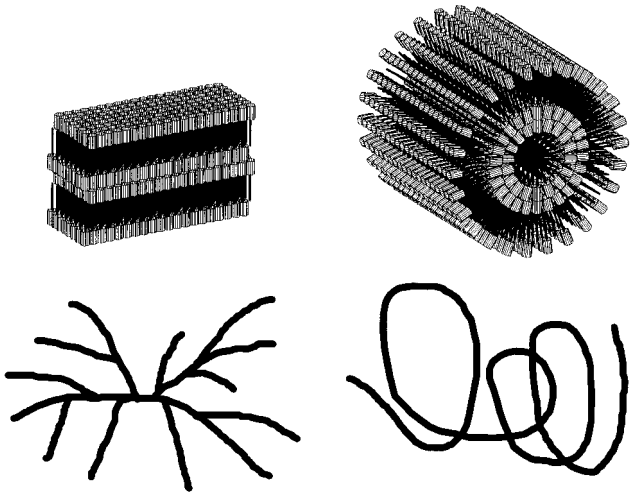

Figure 2. (a, left) Schematic showing one piece of the branched ribbons and the details of a rectangular building brick. (b, right) Schematic showing one piece of the coiled cylindrical fibers and the details of a cylindrical building brick.

$$\tilde{P}(Q) = \frac{V_p^2}{4\pi} \int_{-1}^{1} d\mu \int_0^{2\pi} d\phi \, |A(\vec{Q})|^2 \tag{2}$$

in spherical coordinates (r, θ, ϕ, $\mu = \cos\theta$), where V_p is the volume of the particle and

$$A(\vec{Q}) = \frac{1}{V_p} \int_{V_p} d\vec{r} \, (\rho(\vec{r}) - \rho_s) \, e^{i\vec{Q}\cdot\vec{r}} \tag{3}$$

The integration above is a volume integral over one particle, $\rho(\vec{r})$ is the scattering length density of the particle at location $\vec{r}$, and ρ_s is the scattering length density of the solvents.

For both cylindrical and ribbon models, the first step in constructing the mathematical formula is to define the particle for the integration in eq 3. Therefore, we define the particle by chopping the long fibers, either with a cylindrical cross section or with a rectangular cross section, into smaller building bricks with straight edges. Figure 1 is a two-dimensional schematic representation of the idea of chopping a branched long fiber into small bricks, and each brick has a rectangular shape which facilitates the mathematical modeling.

In the cylindrical model, it is unlikely that the cylindrical fibers can have branches; as a result, there are many very long and coiled cylindrical fibers tangled together to form the networks for the gel. Figure 2b shows one long cylindrical fiber and the details of a cylindrical brick. Figure 2a shows a small section of the branched ribbon structure and the details of a

rectangular brick resulting from the chopping of the structure. The branching in this model can take place on the side of the fibers, which is in the direction parallel to the layers in the crystals. An edge dislocation-like branching similar to that found in phospholipid bilayers[15] is also possible. The repeating distance of the layering structure in both of the models was calculated independently by examining the position of the Bragg peaks in the SAXS scattering data. The result is ~45 Å, which equals twice the length of the fluorocarbon segment of the copolymer plus the length of the hydrocarbon segment of the copolymer. As a result, in both models, the internal structures are fixed with a bilayer arrangement of the copolymers, with fluorocarbon segments closely packed side-by-side and head-by-head and hydrocarbon segments interdigitally stuffed in between the fluorocarbon layers. In order to match two hydrocarbon segments (total area 37 Å^2) to one fluorocarbon segment (area 28.3 Å^2) in this interdigitated packing, either the fluorocarbon segment has to tilt to produce larger cross-sectional area or the perfluorooctane has to be involved in the fluorocarbon part of the packing to fill the empty space. In this section, we are constructing the models on the basis of the second remedy to maintain the 45 Å repeating distance mentioned above.

1. Cylindrical Model. For a cylindrical shape brick with internal structure as described in Figure 2b

$$A(\vec{Q})_{\mathrm{cyl}} = \frac{1}{V_{\mathrm{pcyl}}}\int_{-L/2}^{L/2} \mathrm{d}z\, \mathrm{e}^{iQ_z z} \int_0^{2\pi} \mathrm{d}\theta \int_0^R \mathrm{d}r \times r[\rho(r) - \rho_s]\mathrm{e}^{iQ_\perp r\cos(\theta)}$$

$$= \frac{\sin(Q_z L/2)}{Q_z L/2}\left\{(\rho_f - \rho_h)\left[\sum_{j=1}^{l}\left(\frac{jt}{R}\right)^2\left(2\frac{J_1(Q_\perp jt)}{Q_\perp jt}\right) - \sum_{j=0}^{l}\left(\frac{jt+H}{R}\right)^2\left(2\frac{J_1(Q_\perp(jt+H))}{Q_\perp(jt+H)}\right)\right] + (\rho_f - \rho_s)\left(2\frac{J_1(Q_\perp R)}{Q_\perp R}\right)\right\} \quad (4)$$

where $V_{\mathrm{pcyl}} = \pi R^2 L$ is the volume of the cylindrical brick, $t = 2F + H$ is the thickness of one bilayer, F and H are the lengths of fluorocarbon and hydrocarbon segments of a F_8H_{16} molecule respectively, L is the length of the cylinder, $R = (l + 1)t - F$ is the cross-sectional radius of the cylinder, l is the number of bilayers in the radial direction, and ρ_f and ρ_h are scattering length densities of fluorocarbon and hydrocarbon respectively. $Q_z = Q\mu$ is the component of $\vec{Q}$ in the axial direction, and $Q_\perp = Q(1 - \mu^2)^{1/2}$ is the component of $\vec{Q}$ in the cross-sectional plane.

In spite of the fact that the bricks are connected to each other to form the long fibers and are not allowed to rotate freely, by assuming randomly distributed fibers in three-dimensional space, the resulting building bricks are indeed uniformly distributed in all the directions with respect to Q. Thus we can use eq 2 to calculate the rotation-averaged particle structure factor. We apply eq 4 to eq 2 and calculate the rotation-average particle structure factor by doing numerical integration. Before we can use eq 1 to calculate the absolute scattering intensity, we need to find out the particle number density for this model, which can be done by using the equation $n_{\mathrm{pcyl}} = \eta_{\mathrm{cyl}}/V_{\mathrm{pcyl}}$, where η_{cyl} is the volume fraction of cylindrical bricks in the sample. The adjustable variables in this model include L, l, and η_{cyl}. ρ_s can be derived by subtracting the amount of F_8H_{16} which forms crystals from the known total concentration of F_8H_{16} in the sample.

2. Ribbon Model. In this case a rectangular brick with internal structure as shown in Figure 2a has length L, width W, and thickness nt, where n is the number of bilayers. The volume of a single brick $V_{\mathrm{prib}} = nLWt$, $n_{\mathrm{prib}} = \eta_{\mathrm{rib}}/V_{\mathrm{prib}}$ where η_{rib} is the volume fraction of the rectangular bricks, and

$$A(\vec{Q})_{\mathrm{rib}} = \frac{1}{nLWt}\int_{-L/2}^{L/2} \mathrm{d}x\, \mathrm{e}^{iQ_x x} \int_{-W/2}^{W/2} \mathrm{d}y\, \mathrm{e}^{iQ_y y} \int_{-nt/2}^{nt/2} \mathrm{d}z \times [\rho(z) - \rho_s]\mathrm{e}^{iQ_z z}$$

$$= \frac{1}{nt}\frac{\sin(Q_x L/2)}{Q_x L/2}\frac{\sin(Q_y W/2)}{Q_y W/2}\left\{2F(\rho_f - \rho_s) \times \left\{\cos\left(Q_z\frac{nt - F}{2}\right)\frac{\sin(Q_z F/2)}{Q_z F/2} + 2\left[\frac{n-1}{2} - m + \sum_{j=1}^{m}\cos\left(Q_z\frac{n-2j}{2}t\right)\right]\frac{\sin(Q_z F)}{Q_z F}\right\} + 2H(\rho_h - \rho_s)\left[\frac{n}{2} - m + \sum_{j=1}^{m}\cos\left(Q_z\frac{n+1-2j}{2}t\right)\right]\frac{\sin(Q_z H/2)}{Q_z H/2}\right\} \quad (5)$$

where $m = n/2$ for even n, $m = (n - 1)/2$ for odd n. $Q_x = Q(1 - \mu^2)^{1/2}\cos\phi$ is the component of $\vec{Q}$ along the length of the brick, $Q_y = Q(1 - \mu)^{1/2}\sin\phi$ is the component of $\vec{Q}$ along the width of the brick, and $Q_z = Q\mu$ is the component of $\vec{Q}$ in the direction perpendicular to the layers. The calculation of absolute scattering intensity can be carried out following the same steps as in the cylindrical model. L, W, n, and η_{rib} are the adjustable variables in this model.

Liquid Part. The liquids in our sample are homogeneous mixtures of four components as mentioned above. This micellar model of the liquids has been described in great detail in a previous paper.[1] Briefly speaking, the micelle is an aggregate of ~20 monomers packed in the same way as in the ribbon model for the crystals. It has a cylindrical shape with fluorocarbons at both ends of the cylinder and hydrocarbons at the center. The length of the cylinder equals the repeating distance of the lamellar layers in the crystalline fibers, and the radius depends on the aggregation number. We use a sticky-hard-sphere model[16] to approximate the interaction between isotropically distributed cylindrical micelles. The variables in the micellar model are R, the radius of the micelle, and a and τ, the effective diameter and stickiness in the interaction model. These micelles serve as the seeds for the growth of long and branched ribbon-like crystalline fibers as we decreased the temperature below the liquid−gel transition temperature. It combines with the ribbon model to give an integral description of the system in both liquid and gel phase.

This micellar model gives satisfactory results compared to the scattering data for low concentration of micelles in the liquids, but it fails at high concentration of micelles, due to the more complicated interaction among the micelles where a simple two-body spherical model such as the sticky-hard-sphere model does not apply anymore. Therefore, we can use this model to analyze the low-concentration liquid phase data or combine the model with ribbon model to analyze the low-concentration gel phase data. This model is also applicable to the high-concentration gel phase data if the micelle concentrations in the entrapped liquids are sufficiently low. Those data sets with $\phi_{\mathrm{COP}} = 0.6$ at 20 and 30 °C fall into that category since at those temperatures, the sample is far into the gel phase, and most of the copolymers are included in the fiber networks, so there are much less monomers left in the entrapped liquid to form micelles.

For the data set that the micellar model doesn't apply to, we use the measured scattering curve, which was taken at higher temperature so that the sample was in the liquid phase, as the

empirical curve for the scattering of the micelles. For example, for the sets of data with $r_v = 0.81$ and $\phi_{COP} = 0.6$, at 40 °C, the sample was in its liquid phase, and at 30 °C the sample became a gel. Therefore, we used the scattering curve at 40 °C, with an adjustment amplitude factor to correct for the volume difference, as the background of the scattering curve at 30 °C and used the cylindrical or ribbon model to calculate the scattering of the crystalline fibers. This data set is the only one we analyzed with the cylindrical model because the micellar model for the liquid is in fact the counterpart of the ribbon model. The counterpart of the cylindrical model doesn't exist.

The combined total absolute scattering intensity can be written as

$$I_{total}(Q) = C\left[(1-\eta)I_{liq}(Q) + \frac{\eta}{V_p}\tilde{P}(Q)\right] \qquad (6)$$

where C is an adjustable constant to account for the possible volume expansion of the sample cells which were under high vacuum during the scattering experiment, and it also accounts for the decrease of the sample volume due to the formation of the gel. Since the center of the sample cell is the last position where the temperature reaches the set value, the formation of the gel inside the cell always produces a small empty space at the center of the cell, where the X-ray beam goes through. The fraction of empty space at the location of the X-ray beam is not controllable. $I_{liq}(Q)$ is the absolute scattering intensity of the entrapped liquid; it can be calculated using the micellar model or can be the empirical number obtained at higher temperature where the sample is in its liquid phase. η is the volume fraction of the crystals in a gel, V_p is the volume of a single brick, and $\tilde{P}(Q)$ is the particle structure factor for either cylindrical model or ribbon model.

Results and Discussions

In this section, we first compare the results of data analyses using cylindrical and ribbon models. Then we summarize the data analyses of all the data sets using the ribbon model, and from the variables extracted in the data analyses section, we suggest a mechanism for the formation of the gel. Least-squares fitting is our criterion in comparing the calculation to the experimental data. The absolute intensity is included in the comparison which imposes a great constraint in the data-fitting process.

Comparison. We used the data set of the sample with $r_v = 0.81$ and $\phi_{COP} = 0.6$ at 30 °C for the comparison between cylindrical and ribbon models. As described in the previous section, for the data analysis for this particular set of scattering curve, we used the same sample at 40 °C as background scattering which actually came from the scattering of the micelles in the entrapped liquid. The results are displayed in Figure 3.

The ribbon model gives much better agreement at the small Q regions; see Figure 3d. The discrepancies for both models at Q ranging from 0.05 to 0.12 Å^{-1} come from the liquid data shown in Figure 3b, which doesn't completely represent the scattering of the micelles for the gel phase data in Figure 3d. For the sharp peak in the experimental data, the ribbon model apparently fits the data better than the cylindrical model. Parts a and c of Figure 3 display the calculations of the cylindrical model and the ribbon model, respectively; the ribbon model produces a major sharp peak that matches the data better than the split peaks produced by the cylindrical model. The ribbon model indicates the brick is 966 Å long and the concentration of the ribbons is 5%, which are more appropriate numbers for the approximation of treating the brick as an independent particle in eq 1 than those numbers given by the cylindrical model, 80 Å and 15%. For the approximation of independent particle to be valid, the interaction between particles needs to be very weak or long ranged. For the situation in our samples, the bricks are essentially connected to each other, and interaction is strong.

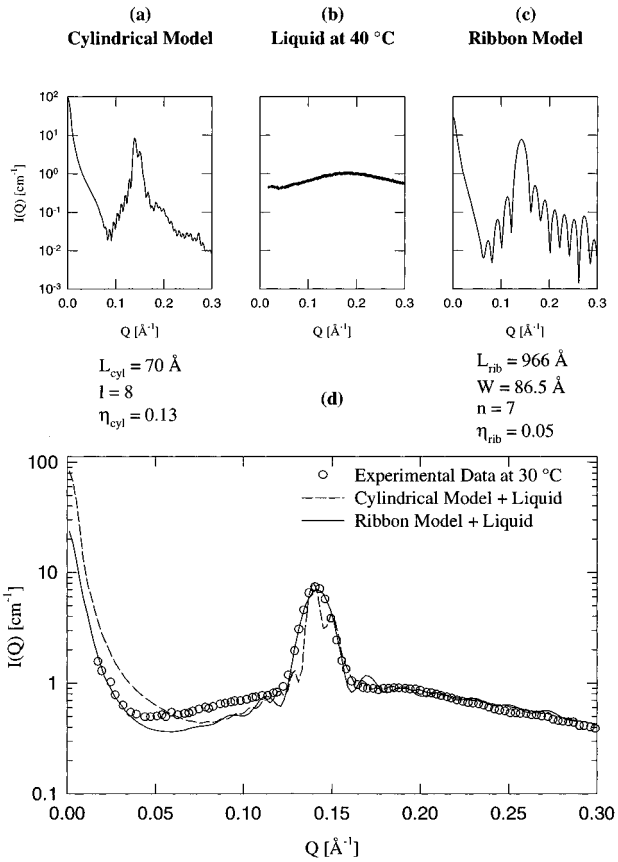

Figure 3. Results of the data analyses of using two different crystalline models. (a) Calculation of the cylindrical model. The numbers below the plot are the extracted variables for the model. (b) Liquid phase data for the micelle scattering. (c) Calculation of the ribbon model. (d) The 30 °C data set of $r_v = 0.81$, $\phi_{cop} = 0.6$ and the resulting curves of combining different models with the micelle scattering of plot b.

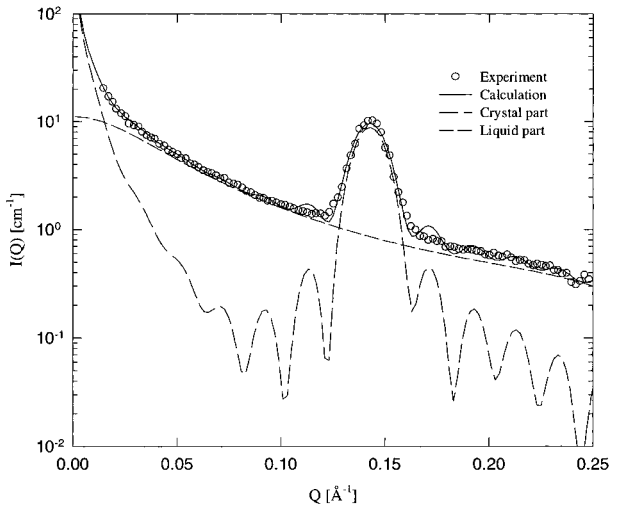

Figure 4. Comparison between the experimental data and the calculations. Open circles are the experimental data points for the sample with 26% F_8H_{16} and $r_v = 2.9$ at 10 °C. The long dashed line is the calculation of the crystal part calculation, the short dashed line is the liquid part calculation, and the solid line is the combination of them.

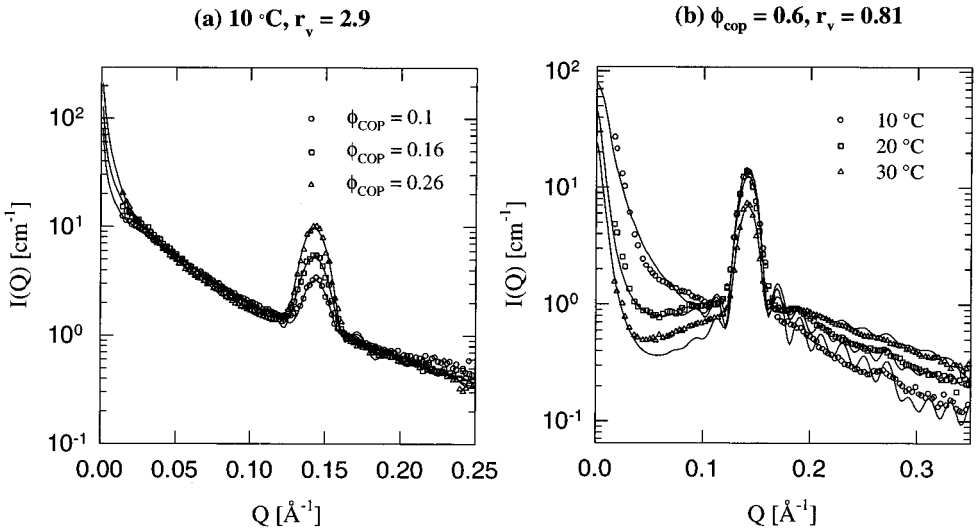

Figure 5. Results of data analyses using the combination of ribbon model for the crystal and micellar model for the liquid. Solid lines are theoretical calculations. (a) Results of three lower ϕ_{cop} samples at the same temperature. (b) Results of one high ϕ_{cop} sample at three different temperatures.

But if the particles were very long, so that the interaction between particles only affects the calculation at very small Q, the approximation is still applicable. For a 966 Å long brick in our case, the effect of interparticle interaction is mostly on $Q < 2\pi/966$ Å $= 0.0065$ Å^{-1}, which is much less than the first Q position in our data.

The comparison above encouraged us to use the ribbon model to continue the data analyses with the rest of our data sets.

Data Analyses. We used the ribbon model combined with the micellar model to analyze the rest of the data sets. Figure 4 is an example of the comparison between the experimental data and calculation. It also displays the crystal part and liquid part of the calculation. The crystal part produces the small-Q peak and the diffraction peak around $Q = 0.14$; the liquid part constitutes the smooth portion of the scattering curve. The multilayer structure of the building brick in our ribbon model also produces oscillations at all Qs as depicted in the figure. These oscillations are not significant for the data sets with relatively low F_8H_{16} volume fractions, namely, the data sets with F_8H_{16} volume fractions of 0.1, 0.16, and 0.26 respectively. Figure 5a displays the results of the data analyses for the samples of $r_v = 2.9$ and three different F_8H_{16} volume fractions at 10 °C. The agreements between the experimental data and calculations are satisfactory. The oscillations will dominate the scattering curve as the crystals dominate the structure of the gel. Figure 5b displays the results of the data analyses for the sample of $r_v = 0.81$ at three different temperatures with a F_8H_{16} volume fraction equal to 0.1. The sample at 10 °C has most crystals and least liquids; therefore, the oscillations are most severe in its theoretical calculation. Another reason for the worse fitting in Figure 5b is the breakdown of the liquid model for high ϕ_{COP} samples as explained in a previous section. One of the possible solutions for the oscillations in the calculation is the incorporation of diffuse boundaries between layers and the polydispersed layer thickness. Another possibility is to have a polydisperse particle system instead of the monodisperse system in use in this article. Either approach will involve a lot more computation in the data analysis process.

Table 1 summarizes the variables extracted from the data analyses. It is interesting that the building brick or the unit cell in our crystal model has seven or eight bilayers, which corresponds to 300−350 Å, and it is very long but extremely narrow. The size of the building brick varies with concentration and temperature. It is longer and narrower at low concentration and becomes shorter and wider at high concentration. On the other hand, it is longer and narrower at higher temperature and shorter and wider at lower temperature. The fibers constructed by longer building bricks are less curly than the fibers constructed by shorter bricks. For the micelle part of the variables, the size of the micelles remains approximately the same and they have similar stickiness regarding the interaction among them. The special case is the data set of $\phi_{COP} = 0.6$, $r_v = 0.81$ at 20 °C. The micellar model is about to break down in this case.

TABLE 1: List of Variables Extracted from the Data Analyses for Different Samples

r_v	ϕ_{COP}	temp (°C)	L	W	n	η	ϕ'_{COP}[a]	R	a	τ
2.9	0.1	10	3150	13.6	8	0.024	0.076	9.08	23.3	0.082
	0.16		2900	41.1	7	0.027	0.133	9.97	27.4	0.106
	0.26		2097	60.6	7	0.063	0.197	9.66	27.3	0.113
0.81	0.6	10	442	121	7	0.425	0.175	9.85	30.6	0.103
		20	913	90.1	7	0.107	0.493	7.41	31.8	9.63
		30	966	86.5	7	0.051	0.549			

[a] ϕ'_{COP} is the volume fraction of F_8H_{16} left in the liquid.

Formation of a Gel. As we have mentioned above, the combination of the ribbon model and micellar model for the gel phase is an extension of the micellar model for the liquid phase. They form an integrated description for the whole system, starting at temperature above the liquid−gel transition temperature where the micellar model applies and ending at temperature below the transition temperature where the gel forms and the combined model applies.

Imagine the liquid phase of the system; the liquid is a homogeneous mixture of four components: perfluorooctane, isooctane, F_8H_{16} monomers, and cylindrical micelles formed by F_8H_{16} monomers. As we decrease the temperature in the liquid phase, the radius of the cylindrical micelles will increase and the number of the micelles in the liquid will also increase. When the temperature is lower than the liquid−gel transition temperature, the F_8H_{16} monomers start to attach to the nearest micelles. Due to the particular feature of the micelle, it is easier for the monomers to attach to the micelle from the radial direction than from the axial direction. At the beginning, the micelle starts to grow uniformly in the radial direction, and after a while, there are random positions around the peripheral of the micelle that catch more monomers than other positions. These positions form islands around the micelle and deplete the nearest monomers around the micelle at the moment. The tips of these

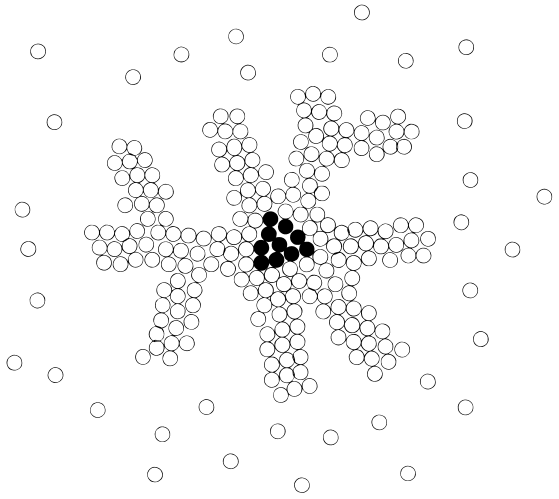

Figure 6. Two-dimensional schematic of the growing of the crystalline matrix (ribbons) of a gel.

islands are now the closest positions for the monomers surrounding the micelle to attach to; therefore, these islands grow toward the solvent and become strips. Each strip may split into two strips due to the increasing peripheral area for cylindrical geometry as the radius increases. As the strip grows longer, the monomers can also slowly attach to the strip along the axial direction so as to make the strip thicker. The width of a strip is limited by the competition of neighboring strips. At the end of the formation process, according to the results of the data analyses, these strips become long, curly ribbons with the thickness corresponding to the width of the strips and the width corresponding to the thickness of the strips. Figure 6 is a two-dimensional schematic drawing (top view) of a growing structure just described. The final shape of the ribbons depends on the concentration and temperature of the sample as described in the data analyses section. It is reasonable that at lower concentration there are less seeds to start the growing of a gel; therefore, there is less interference on the growing of the ribbons, which makes the ribbons less curly. Due to the fact that there are less monomers in the solvent, the ribbons are thinner. It is unlikely to have edge dislocation-like branches as mentioned above for the ribbons formed following the description above.

In the entrapped liquids among these ribbons, there are monomers and micelles. Each micelle is constructed by $\approx$20 monomers. These micelles may be the micelles from the liquid phase which fail to grow, or they may be formed during the gel formation process. They keep the mixture of isooctane and perfluorooctane from phase separation. Table 1 lists the volume fractions of ribbons in the samples and the remaining F_8H_{16} in the liquid. The second set of numbers all exceed the corresponding thresholds of having homogeneous mixtures as mentioned in the models of the gel section. It verifies the entrapped liquids are indeed one-phase liquids.

Conclusions

The presence in the same molecule of two incompatible units produces peculiar phenomena such as supramolecular aggregation in selective solvents. We report a SAXS study on the structure of the micelles and gels formed by a diblock semi-fluorinated alkane, F_8H_{16}, in a solvent constituted by a mixture of perfluorooctane and isooctane.

In this paper, we investigate two models: cylindrical model and ribbon model, for the microstructure of the gel phase of F_8H_{16} dissolved in a mixture of perfluorooctane and isooctane. By analyzing a SAXS absolute intensity curve with both models, we conclude that the ribbon model is the better representation for our samples.

Using a combined model of the ribbon for the crystal part and the micellar model for the liquid part of the gel, we find the fibers in a gel are ribbons with widths of 300−350 Å, thicknesses of 13.6−121 Å, and persistent lengths of 442−3150 Å, depending on the volume ratio of perfluorooctane to isooctane, the volume fraction of F_8H_{16}, and the temperature. Within the persistent lengths, the ribbons are practically straight. We also verify that the entrapped liquids among the fibers are one-phase liquids composed of perfluorooctane, isooctane, F_8H_{16} monomers, and micelles.

From the structural parameters obtained in the data analyses, we propose a growing mechanism for the formation of the gel starting from the liquid phase of a sample. This mechanism gives a reasonable explanation for the final shape of the crystalline fibers in the gel phase.

The models used in this article are approximations of a very complicated system. These calculations include two-dimensional integration; therefore, the data analyses process is rather time consuming. As mentioned in the data analyses section, it is possible to improve the ribbon model by including polydispersed layer thickness, etc. However, these additional improvements will result in extremely cumbersome computations. Even at the present level of the model, the overall agreement with absolute intensity data is good enough to warrant serious consideration.

Acknowledgment. P. Lo Nostro thanks the "Consorzio per lo Sviluppo dei Sistemi a Grande Interfase" (C.S.G.I.) for partial financial support.

References and Notes

(1) LoNostro, P.; Ku, C. Y.; Chen, S. H.; Lin, J. S. *J. Phys. Chem.* **1995**, *99*, 10858−10864.
(2) LoNostro, P. *Adv. Colloids Interface Sci.* **1995**, *56*, 245−287.
(3) Höpken, J.; Möller, M. *Macromolecules* **1992**, *25*, 2482.
(4) Hoyle, C. E.; Kang, D.; Jariwala, C.; Griffin, A. C. *Polymer* **1993**, *34*, 3070.
(5) Höpken, J.; Pugh, C.; Richtering, W.; Möller, M. *Makromol. Chem.* **1988**, *189*, 911.
(6) Dorset, D. L. *Macromolecules* **1990**, *23*, 894.
(7) Percec, V.; Tomazos, D.; Feiring, A. E. *Polymer* **1991**, *32*, 1897.
(8) Rabolt, J. F.; Russell, T. P.; Twieg, R. J. *Macromolecules* **1984**, *17*, 2786.
(9) Russell, T. P.; Rabolt, J. F.; Twieg, R. J.; Siemens, R. L.; Farmer, B. L. *Macromolecules* **1986**, *19*, 1135.
(10) Viney, C.; Russell, T. P.; Depero, L. E.; Twieg, R. J. *Mol. Cryst. Liq. Cryst.* **1989**, *168*, 63.
(11) Höpken, J. Fluorocarbon-Hydrocarbon Mixtures. Ph.D. Thesis, University of Twente, The Netherlands, 1991.
(12) Turberg, M. P.; Brady, J. E. *J. Am. Chem. Soc.* **1988**, *110*, 7797.
(13) Lo Nostro, P.; Chen, S. H. *J. Phys. Chem.* **1993**, *97*, 6535.
(14) Gaines, G. L. *Langmuir* **1991**, *7*, 3054.
(15) Kléman, M.; Williams, C. E.; Costello, M. J.; Gulik-Krzywicki, T. *Philos. Mag.* **1977**, *35*, 33−56.
(16) Ku, C. Y.; Chen, S. H.; Rouch, J.; Tartaglia, P. *Int. J. Thermophys.* **1995**, *16*, 1119−1134.